In situ x-ray studies of native and Mo-seeded surface nanostructuring during ion bombardment of Si(100)

2009 J. Phys.: Condens. Matter 21 224008

(http://iopscience.iop.org/0953-8984/21/22/224008)

IOP Publishing Journal of Physics: Condensed Matter

J. Phys.: Condens. Matter **21** (2009) 224008 (9pp) doi:10.1088/0953-8984/21/22/224008

In situ x-ray studies of native and Mo-seeded surface nanostructuring during ion bombardment of Si(100)

G Ozaydin-Ince[1] **and K F Ludwig Jr**

Department of Physics, Boston University, Boston, MA 02215, USA

Received 5 January 2009
Published 12 May 2009
Online at stacks.iop.org/JPhysCM/21/224008

Abstract

Native and Mo-seeded nanostructuring of the Si(100) surface during Ar^+ ion bombardment is investigated by means of real-time grazing-incidence small-angle x-ray scattering and atomic force microscopy. During off-axis bombardment at room temperature, the native early-stage growth kinetics of nanoripples on the surface is found to be in reasonable overall agreement with theoretical predictions, particularly when an ion impact induced lateral mass redistribution term is included. For normal-incidence bombardment at room temperature, a native short wavelength smoothing of the amorphized Si surface is observed, suggesting that ion impact induced lateral mass redistribution dominates the Bradley–Harper instability. During 5% Mo-seeded normal-incidence bombardment at temperatures up to 450 °C, nanodots form with heights decreasing as the substrate temperature increases. This trend is counter to that typically observed for the growth of large cone structures on metals and suggests that the primary effect of thermal energy here is in promoting surface smoothing, rather than increasing diffusion of seed atoms to form protective clusters. During seeded bombardment at 650 °C the surface remains crystalline and surface corrugations exhibit dynamic scaling characteristic of surface diffusion-driven instabilities. This is the same behavior as is found in the absence of seeding and its presence suggests that at this concentration seeding does not play a large role during normal-incidence bombardment of the Si surface at high temperatures.

(Some figures in this article are in colour only in the electronic version)

1. Introduction

Since at least 1942 it has been known that simultaneous ion bombardment and deposition of trace impurities ('seeding') can lead to the formation of well-defined surface structures on metal targets [1]; these are typically on the micron size scale. More recently, attention has focused on nanostructured morphology development during seeding of semiconductor targets. However, understanding seeding behavior during ion bombardment of semiconductors is complicated by our incomplete understanding of their 'native' behavior, i.e. their behavior in the absence of seeding [2]. For the particular case of Si substrates, the target examined in this work, studies of the native surface evolution at room temperature have reported that low-energy normal-incidence Ar^+ bombardment causes nanodot formation [3–5], or that it does not [6]. Experiments find that off-axis bombardment creates ripples [7, 8], but some report that there is a window of incident angles over which the surface remains smooth [4]. Moreover, there is increasing realization that inadvertent seeding at low levels can significantly influence the surface morphology development [6, 9, 10]. In order to better understand these issues, this work examines both the native and seeded bombardment of Si using real-time grazing-incidence small-angle x-ray scattering (GISAXS) and atomic force microscopy (AFM).

Many semiconductors are amorphized by ion bombardment at room temperature. For amorphous materials, theoretical understanding of native surface behavior during ion bombardment is usually based on the Bradley–Harper (BH) model [11], in which an amorphous plane surface is unstable to height fluctuations, a consequence of Sigmund's theory [12] of sputter erosion. The BH theory makes well-defined predic-

[1] Present address: Department of Chemical Engineering, MIT, Cambridge, MA 02139, USA.

tions for the magnitude of the curvature instability though experiments have typically reported somewhat larger values than predicted by theory [2]. In the BH theory, competition between curvature-driven instability and relaxation produces a maximum surface structure growth at an intermediate wavenumber $q_{\max}$. Studies have found that the dependence of $q_{\max}$ on angle of bombardment, temperature, ion energy and/or ion flux are consistent with BH expectations in the early stages of bombardment (i.e. before nonlinearities dominate the surface evolution) [13, 7]. Further complicating the picture are observations that ripples move in the direction opposite to that predicted by the BH approach [14], possible effects of non-Gaussian response functions [15, 16] and ion impact induced lateral mass redistribution [17–19], which can smoothen amorphous surfaces during normal-incidence bombardment.

To better clarify the native relaxation on Si surfaces during low-energy Ar^+ bombardment, we begin these experiments by examining the GISAXS structure factor evolution, which allows the unambiguous extraction of the key instability and relaxation parameters predicted by theory for off-axis bombardment. Trying to directly study the effects of normal-incidence bombardment without seeding can be challenging since small amounts of inadvertent seeding from material sputtered from other parts of the environment onto the sample can potentially play a dominant role. We therefore examine the evolution of a nanostructured sample during normal-incidence bombardment—i.e. investigate whether the bombardment inherently smoothens the surface on short length scales. We find that such ripples *are* smoothened by the bombardment, as has also been observed for sapphire and silica [19].

After examining the native Si surface behavior during bombardment, we consider Mo-seeded morphology development on Si(100). The fundamental mechanisms involved in nanostructure development during seeding on different materials are still unclear. In their study of Cu target bombardment with Mo seeding, Wehner and Hajicek [20] suggested that seed atoms migrate on the surface to form regions of relatively high seed concentration. If these regions have a lower sputter yield than the substrate material, they could protect areas below them and form nucleation sites for the cones. Further growth of the cones relative to the surrounding material in this scenario is due to continued migration of the seed atoms to the cones and protection of the underlying material. A different approach was articulated by Begrambekov *et al* [21] based upon their study of W seeding of Cu during ion bombardment. According to their theory, as the concentration of seed atoms increases at a point on the surface, the surface stress in that location increases and protuberances form to relieve the stress. In both the Wehner and Hajicek [20] and the Begrambekov *et al* [21] approaches, seed atom migration plays a vital role. Therefore cone growth is typically enhanced at higher temperatures on metals, consistent with the idea that seed migration forms an important part of the cone formation process.

Early studies focused on seeding during ion bombardment of metals. It is only more recently that seeding of Si targets has received significant attention [22–26], particularly the formation of 'nanodots' during normal-incidence bombardment of Si with Mo seeding [6, 27, 28, 9, 10]. These nanodots are typically of order 30 nm in width and 1 nm in height.

Our previous measurements of stress and nanodot growth rate suggest that seed induced stress could play a major role in nanodot formation on Si during seeding [28]. This is somewhat similar to the suggestion of Begrambekov *et al* [21] for metal seed cone formation, but possibly without the need to form concentrated seed atom regions. However, other mechanisms, such as the formation of protected regions, have not been ruled out. Given the results of Tanemura *et al* [26], showing the positive effect of increased temperature in the formation of microrods, and the potentially vital role of seed surface diffusion, it is expected that understanding the temperature dependence of the nanodot formation kinetics may give important clues about the underlying mechanisms at work during seeding of Si. Therefore, to better investigate the nature of the seeding mechanisms at work, this paper examines the temperature dependence of morphology development on Si during Ar^+ bombardment with Mo seeding. The use of real-time x-ray measurements is particularly advantageous for high temperature studies since the surface morphology may change during the cooling process for *post facto* studies.

2. Experiments

Ion bombardment experiments were performed in an ultra-high vacuum (UHV) x-ray diffraction chamber with a base pressure of 10^{-9} Torr. Seeding studies were performed using an Oxford Scientific 'OSPrey' Microwave Plasma Source and ultra-high purity Ar gas. The ion flux of the source was approximately 7 μm^2 at 500 eV, as measured by a Faraday cup. The beam diameter was approximately 3 cm. Si(100) samples were bombarded with 500 eV Ar^+ ions at temperatures ranging from 25 to 650 °C. Mo clips were used to hold the sample; they also acted as the seeding sources. *Post facto* x-ray photoelectron spectroscopy (XPS) measurements show that the concentration of Mo on the Si surface after bombardment is approximately 5%. We have also performed *in situ* reflection high-energy electron diffraction (RHEED) measurements on the samples. As expected, these show that for temperatures below 400 °C, the surface is amorphized. However, above 400 °C a transition region from amorphous to crystalline is observed and at 650 °C the surface remains crystalline.

Our experience is that the Oxford Scientific OSPrey source can inadvertently provide a small stream of seed atoms from its grids. For studies of native Si surface evolution during bombardment, we therefore used a PHI ion gun from Physical Electronic Inc. It is gridless and has an ion flux of 0.54 μm^2 at 1000 eV. The beam diameter of this source is approximately 1 cm.

The real-time x-ray experiments were performed on beamline X21 of the National Synchrotron Light Source (NSLS), at Brookhaven National Laboratory. The GISAXS measurements used a typical incident x-ray angle of 0.8° and an exit angle of 0.2°; the x-ray energy was 11 keV. A custom linear diode array x-ray detector constructed by Dr Peter Siddons of Brookhaven National Laboratory was used to monitor the x-ray scattering. After the ion bombardment, the

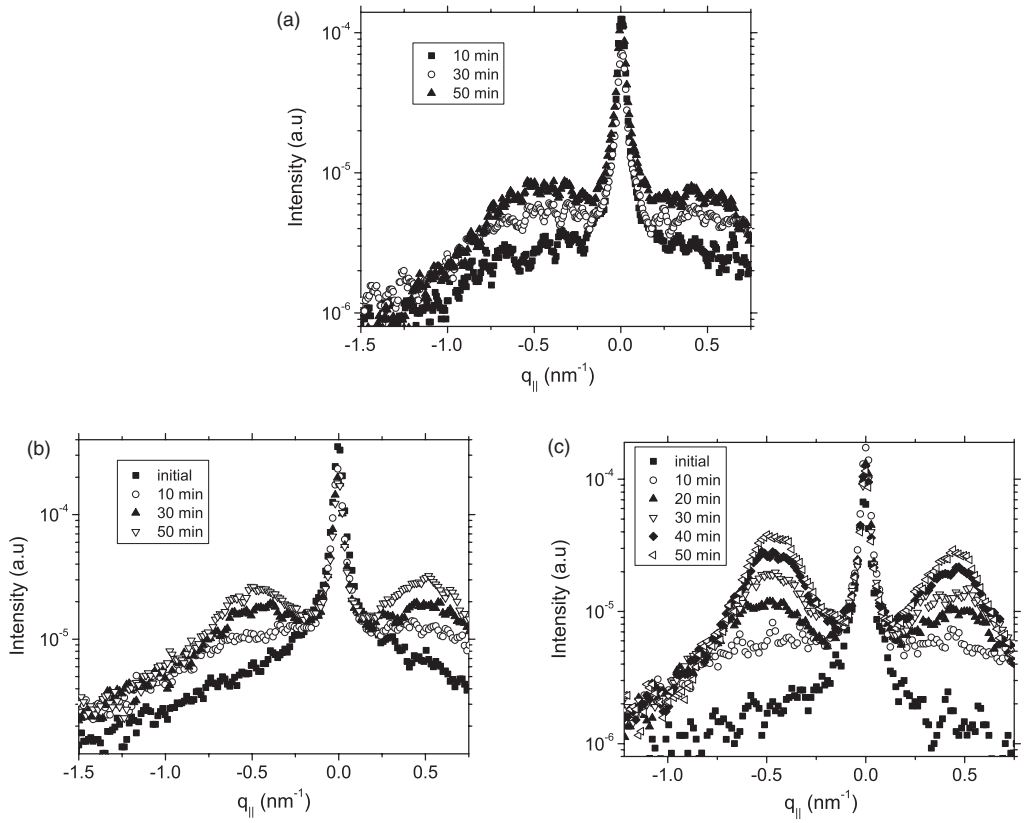

Figure 1. Selected GISAXS scans of the samples bombarded at 1000 eV at ion incidence angles of (a) 45°, (b) 52.5° and (c) 60°.

samples were taken out of the chamber and AFM analysis was performed.

The scattered GISAXS intensity measured is related to the height of the surface $h(x, y)$:

$$I(q_x, q_y, q_z) \propto \left| \frac{1}{q_z} \int \int \mathrm{d}x\, \mathrm{d}y \exp[\mathrm{i}(q_x x + q_y y)] \times \exp[\mathrm{i} q_z h(x, y)] \right|^2 \quad (1)$$

where q_x, q_y, q_z are the Cartesian components of the x-ray photon wavevector change and the z-direction is perpendicular to the sample surface [29]. In the limit $q_z h(x, y) \ll 1$, expansion of equation (1) shows that the measured intensity is proportional to the square of the Fourier transform of $h(x, y)$. We have found that during normal-incidence bombardment, structures forming on the amorphized Si surface are isotropic in the x–y plane, and hence q_x and q_y are equivalent—we can then refer to them as simply $q_\parallel$. Integrating GISAXS intensity over $q_\parallel$ gives the mean-square roughness.

3. Experimental results

3.1. Native surface morphology evolution

3.1.1. Formation of ripples during off-axis bombardment. Silicon (100) surfaces were bombarded with 1000 eV Ar^+ ions at different incidence angles φ away from the surface normal: $\varphi = 45°$, 52.5°, and 60°. Because of the x-ray scattering geometry, the surface morphology evolution could not be measured during the off-axis bombardment process itself. Instead, every 10 min the bombardment was temporarily stopped and the sample was rotated into position for the GISAXS measurement. This bombardment and measurement cycle was repeated five times for each sample corresponding to 50 min of total bombardment. After the ion bombardment, the samples were removed from the chamber and AFM analysis was performed. Measurements showed that the temperature of the sample surface did not increase more than 5 °C throughout the experiments due to the low ion flux of the source. RHEED measurements during and after the bombardment showed that the surface is amorphized during the process.

Figure 1 shows selected GISAXS scans of the samples—the growth of structure factor peaks due to the development of a correlated surface morphology is clearly seen. In the GISAXS orientation used, the ripples examined have a wavevector parallel to the projected ion beam direction. *Post facto* AFM images show the formation of the correlated roughness, but higher fluences than those examined here are required before well-defined ripples are observed. By the time that such ripples are observed in AFM, our experience suggests that nonlinear effects beyond the linear BH description are often observed in the GISAXS evolution.

Before examining detailed fits of the structure factor evolution to linear BH theory, we first consider the overall variation in roughening rate and characteristic wavelength with ion incidence angle. These can be obtained from simple Lorentzian fits of the final GISAXS patterns. The results (figure 2) show that the correlation peak amplitude (and

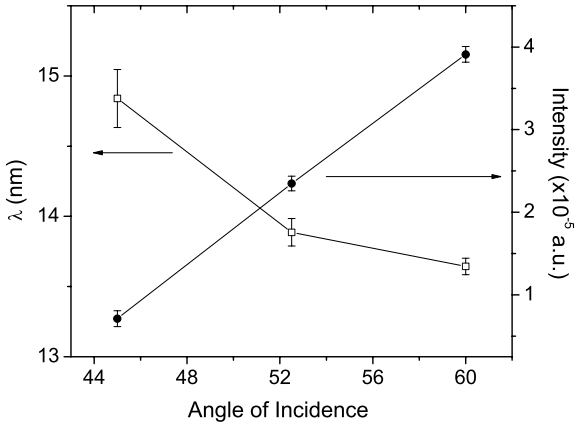

Figure 2. The correlation peak amplitudes and the characteristic wavelengths for different incidence angles after 50 min of bombardment.

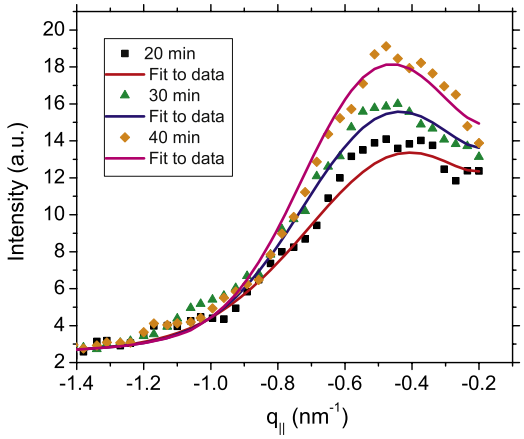

Figure 3. Fits of consecutive GISAXS scans to the modified BH theory of equation (4) for the sample bombarded at 52.5°.

therefore roughening rate) is highest at the largest angles φ examined here. The dominant wavelength on the surface, $\lambda \approx (2\pi/q_{\max})$, decreases somewhat with increasing ion incidence angle.

For a projected ion beam direction along the y-axis, the modified BH linear theory for the change in height h at a given point x, y on the sample is:

$$\frac{\partial h}{\partial t} = -\upsilon_0 + \xi\partial_y h + (\nu_x + \alpha_x)\partial_x^2 h + (\nu_y + \alpha_y)\partial_y^2 h - D_{xx}\partial_x^4 h - D_{yy}\partial_y^4 h - D_{xy}\partial_x^2\partial_y^2 h - (K + B)\nabla^4 h + \zeta(x, y, t). \quad (2)$$

The first term on the right is the average sputter erosion rate which is constant throughout the process. The second coefficient, ξ, is zero for normal-incidence bombardment and determines the ripple velocity for off-normal bombardment. However, it does not affect the structure factor growth [30]. The term $\nu_{x,y}$ is the BH curvature dependent roughening term and $\alpha_{x,y}$ is the lateral mass redistribution term. If $(\nu + \alpha)$ is negative then the surface is unstable to the growth of fluctuation modes with wavenumber in the appropriate x- or y-direction; if it is positive, then the surface is smoothened by ion bombardment. For the studies of nanoripple formation by off-axis bombardment reported in this work, the instability in the y-direction is the dominant mode since this is the projected ion beam direction. In equation (2), K is the ion induced or thermally activated surface diffusion (SD) term. The coefficient B is due to ion-enhanced surface viscous flow (IVF) [31]. The surface erosion smoothing (SES) terms [30], $D_{x,y}$, are due to higher order terms in the expansion of Sigmund's Gaussian expression for ion energy deposition in the material. The noise term in equation (2) has the properties $\langle\zeta(\boldsymbol{r}, t)\rangle = 0$ and $\langle\zeta(\boldsymbol{r}, t)\zeta(\boldsymbol{r}', t)\rangle = nA\delta(\boldsymbol{r} - \boldsymbol{r}')\delta(t - t')$ where A is the surface area.

The theoretical values of ν and D can be calculated from the ion energy deposition depth a, the ion energy distribution widths parallel and perpendicular to the incoming ions beams σ, μ, the ion flux J and the sputter yield $Y(\theta)$ using relations given by Makeev *et al* [32]. The IVF term B is:

$$B = \frac{\gamma d^3}{\eta_s}, \quad (3)$$

where d is the depth of the amorphized layer (typically assumed to be comparable to the ion penetration depth), γ is the surface tension and η_s is the ion-enhanced viscosity of the amorphous surface layer.

For scattering in the y-direction with $q_x = 0$ the linear equation (2) predicts a structure factor evolution:

$$S(q_y, t) = S(q_y, 0)\exp[-2((\nu_y + \alpha_y)q_y^2 + (K + D_{yy} + B)q_y^4)t] + [n/2((\nu_y + \alpha_y)q_y^2 + (K + D_{yy} + B)q_y^4)]\{1 - \exp[-2((\nu_y + \alpha_y)q_y^2 + (K + D_{yy} + B)q_y^4)t]\}. \quad (4)$$

To examine the applicability of the linear model and to obtain the total curvature $(\nu_y + \alpha_y)$ and relaxation $(K + B + D_{yy})$ coefficients, the kinetic evolution of the experimental GISAXS structure factors in the y-direction at each ion incidence angle were fit to equation (4). As seen in figure 3, the fits are good. One point to note is that the full linear theory with noise actually predicts a slight peak shift with time, as is observed in this early regime. Results from the fits are given in table 1.

Table 1. Experimental values of the linear theory coefficients from fits of equation (4) to the GISAXS structure factor evolution.

Ion angle (φ) (deg)	$(\nu_y + \alpha_y)_{\exp}$ ($(\times 10^{-4})$ nm^2 s^{-1})	$(K + D_{yy} + B)_{\exp}$ ($(\times 10^{-3})$ nm^4 s^{-1})
45	-9.1 ± 0.1	2.6 ± 0.3
52.5	-14.0 ± 0.5	3.3 ± 0.2
60	-26.0 ± 0.6	5.9 ± 0.1

As discussed above, using values of a, σ, μ and $Y(\theta)$ from SRIM [33], theoretical values of ν_y can be calculated. The ripples with wavevector in the y-direction should disappear when ν_y becomes positive. However, the calculated values of ν_y become positive for $\varphi > 54°$, in disagreement with the strong ripples we observe forming during 60° bombardment.

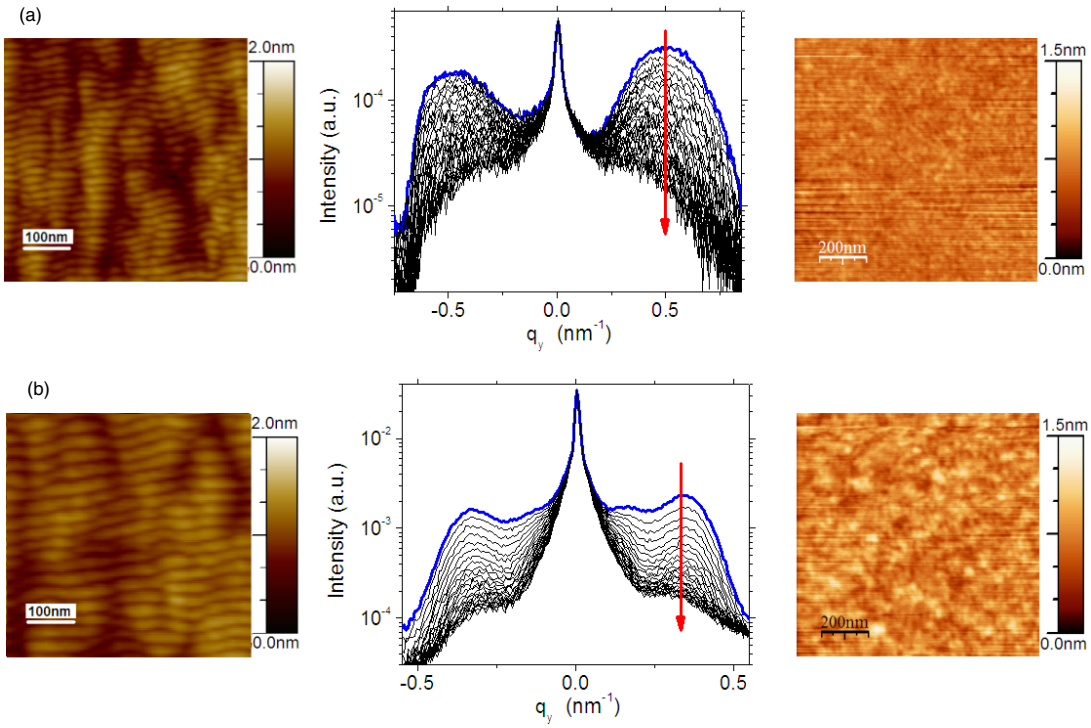

Figure 4. Smoothening of nanoripples during normal-incidence bombardment of Si without seeding. Ion energies are (a) 500 eV and (b) 1000 eV.

Since the SRIM calculations are believed to have limited accuracy at low ion energies and the theoretical values of ν_y and D_{yy} are quite sensitive to the values of a, σ, and μ used in their calculation, we therefore consider only whether the BH coefficients are comparable to those experimentally measured. The calculated instability parameter ν_y is $(1\text{–}2\times10^{-3}$ nm^2 s$^{-1})$ for medium bombardment angles φ. The value of the estimated lateral mass redistribution term α_y can be estimated using SRIM calculations using the method outlined in [19]. The α_y coefficient decreases with increasing ion bombardment angle and is approximately 2.5–4 $\times$ 10^{-4} nm^2 s^{-1} in this angle range. Thus the calculated value for $(\nu_y + \alpha_y)$ is comparable in magnitude to the measured values of the net instability curvature coefficient given in table 1, and we conclude that BH agreement with experiment is reasonable. However, it is noteworthy that the measured coefficient values show a distinct decrease in magnitude with decreasing φ. Since the BH parameter ν_y is relatively constant as normal incidence is approached, this suggests that the lateral mass redistribution term α_y could be playing a somewhat larger role than the estimates made using SRIM would suggest.

SRIM parameters can also be used to estimate the contribution of the SES term D_{yy} to surface relaxation. The SRIM values suggest that this term is of order 1×10^{-3} nm^4 s^{-1} at low angles φ but changes sign at $\varphi \sim 40°$. The overall magnitude is comparable to, but smaller than, that of the experimentally observed sum of relaxation coefficients $(K + D_{yy} + B)$ in table 1. Given the inherent uncertainties in the SRIM parameters entering into the calculation of D_{yy}, it is therefore uncertain whether it is a major contributor or not. Previous studies [19, 31] of amorphized semiconductor and insulator surfaces have concluded that IVF plays a dominant role. If it is assumed that it also plays a dominant role here, equation (3) suggests that the ion-enhanced surface viscosity η_s is of order 10^{12} Pa s. This is 3 orders of magnitude larger than the value observed for the bombardment of sapphire in [19]. However, the ion flux in that work was approximately 3 orders of magnitude larger than that used here. Therefore, η_s approximately varies in inverse proportion to the ion flux, as expected if ions excite local configurations allowing viscous relaxation.

3.1.2. Nanoscale smoothing of ripples during normal-incidence bombardment. To prepare starting samples for these studies, Si(100) surfaces were first bombarded at 45° off-normal incidence with 500 and 1000 eV Ar^+ ions from the PHI ion gun at room temperature to form nanoripples. The surfaces were then bombarded with normal incidence Ar^+ ions from this source at room temperature; the ripples formed at 500 eV were bombarded at normal incidence with 500 eV ions and the ripples formed at 1000 eV were bombarded with 1000 eV ions.

Figure 4 shows the real-time GISAXS scans during the smoothing of the ripples by 500 and 1000 eV ion bombardment and initial and final AFM images of the surface. The consecutive GISAXS scans of normal-incidence ion bombardment are approximately 135 s apart. As seen in the GISAXS scans, correlation peaks are initially observed on each side of the specular peak, corresponding to the formation of ripples after off-normal ion bombardment. The initial GISAXS scans are marked in blue in figure 4 and the decay of the intensities is shown with an arrow. As seen in the figure, the intensities of the correlation peaks on both sides

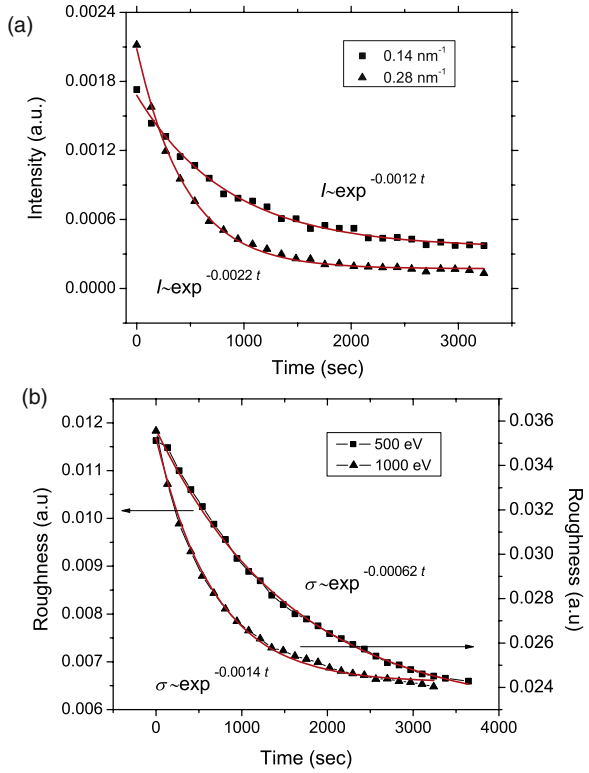

Figure 5. (a) Smoothening of nanoripple structure factor at two different wavenumbers, (b) smoothing of overall surface roughness. Lines are exponential decay fits.

of the specular peak decreased with time during normal-incidence bombardment and at later times, the correlation peaks almost completely disappear. This behavior is also seen in the AFM images of figure 4; before the bombardment at normal incidence the ripples can be seen clearly, however, after the bombardment they are completely eroded and only a background roughness is observed for both energies.

The time evolution of the GISAXS intensities at two different wavenumbers is plotted in figure 5(a) for 1000 eV. As seen in the figure, the intensities in the high-q region decay faster than the low-q region, showing that the short length scale ripples decay faster than the large length scale ripples. Figure 5(b) shows the decay of roughness in time for 500 and 1000 eV, where the roughness values are calculated by integrating the GISAXS intensities. As discussed above, the accuracy of calculating ν_y from SRIM parameters is limited. However, given the overall smoothing behavior of normal-incidence bombardment, it appears likely that here the ion induced lateral mass redistribution is larger than the BH instability.

3.2. Mo-seeded surface morphology evolution

3.2.1. Qualitative features. Figure 6 shows the real-time evolution of GISAXS scans during normal-incidence Mo-seeded bombardment at different substrate temperatures, as well as *ex situ* AFM images of the same samples after bombardment and cooling. The consecutive GISAXS scans are approximately 3 min apart. As can be seen in figure 6, the overall GISAXS scans look similar for temperatures below 450 °C. Well-defined peaks are seen to form due to the growth of correlated structures, i.e. nanodots, on the surface. The correlated nanodots can be clearly seen in the AFM images. In addition to the nanodots, a large length scale (~100 nm) background roughness is also observed in the AFM images. This kinetic roughening corresponds to the shoulder peaks observed on both sides of the specular peaks of the GISAXS scans. As the temperature is increased, a transition region is observed where the GISAXS scans show a different behavior and the dots are no longer visible. At 650 °C, formation of a rapidly coarsening correlated roughness is observed; it is distinctly different than the low temperature behavior, but similar to what we have observed at high temperatures in the absence of seeding [34]. Since our RHEED measurements indicate that the surface remains crystalline at 650 °C, we analyze the data from this temperature separately.

3.2.2. Analysis of structure evolution—temperatures below 650 °C. To better characterize the evolution of the short wavelength sample morphology, the correlation peaks in the GISAXS scans were fit to a heuristic function—a modified Lorentzian squared: $\{2Awq_\parallel/[4\pi(q_\parallel - q_0)^2 + \pi w^2]\}^2$, where A, w and q_0 are fit parameters related to the peak position, $q_{\max} = \sqrt{4q_0^2 + w^2}/2$, and the peak amplitude, $A_{\max} = \{2Awq_0/[4\pi(q_m - q_0)^2 + \pi w^2]\}^2$. From these fits the time evolution of the lateral length scales and the correlation peak intensities can be obtained as seen in figure 7. For temperatures in the range 25–350 °C the characteristic wavenumbers q_0 of the nanodots relax approximately to ~0.2 nm^{-1} (corresponding to wavelengths of approximately 30 nm) as ion bombardment continues (figure 7(a)). The final characteristic length scales in this range do not show significant temperature dependence. At 450 °C, on the other hand, the nanodots disappear but a correlated roughness of wavelength of about 20 nm forms. At 550 °C the correlation peaks do not grow as much as at lower temperatures and they show complex behavior, thus the fits of this temperature are omitted here.

Figure 7(b) shows the evolution of the amplitudes of the correlation peaks obtained from the fits. At all temperatures there is a rapid initial increase of the amplitudes, but at later times the growth slows and the amplitude saturates for all temperatures except 650 °C. At temperatures lower than 650 °C, the overall behavior of the amplitude evolution is that the saturation amplitude decreases as the temperature increases.

The average nanodot heights formed by ion bombardment at temperatures 25–450 °C can be found from the q_z dependence of the GISAXS data (not shown here). A fit of the function $f(q_z) = q_z^2\theta I(q_z)$ (where the factor of θ, the x-ray angle of incidence, arises from the scattering geometry), to a function $A + B\sin^2(q_z h)$ gives an estimate of surface structure height h [27]. In the temperature range 25–450 °C, the average heights of the nanodots at the end of the bombardment process range from 0.8 to 1.7 nm as shown in figure 8. Above 450 °C nanodot formation is not clearly visible.

The integrated GISAXS intensity is proportional to the mean-square surface roughness. Figure 9(a) shows the overall

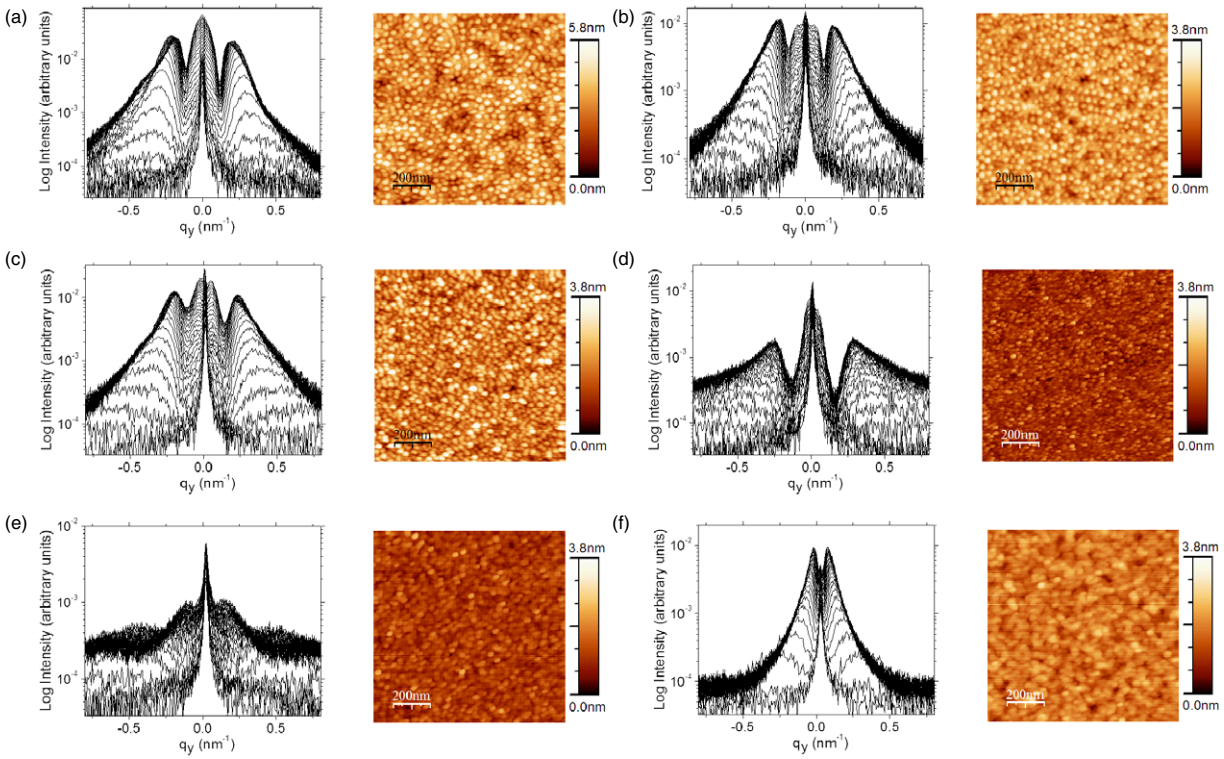

Figure 6. Real-time GISAXS scans and *ex situ* AFM images of samples bombarded at 500 eV at (a) 25 °C, (b) 250 °C, (c) 350 °C, (d) 450 °C, (e) 550 °C and (f) 650 °C.

root-mean-square roughness evolution of the samples as a function of temperature. For temperatures below 650 °C the roughness initially grows superlinearly. After a crossover time, the growth rate decreases and the roughness starts growing almost linearly. As the temperature increases the overall final roughness generally decreases, a trend reflected in the *post facto* AFM measurements of figure 9(b) as well.

3.2.3. Analysis of the 650 °C data. The evolution of the GISAXS structure factor at 650 °C, where the Si surface remains crystalline, is shown in figure 10. It is qualitatively different from that observed at lower temperatures, but is similar to that observed at comparable temperatures in the absence of seeding [34]. On crystalline surfaces some surface diffusion processes such as step-edge diffusion barriers and fast-edge diffusion [35] can lead to surface roughening. These diffusion-mediated instabilities typically produce rapid power law coarsening of the characteristic lateral length scale and power law growth of the overall roughness. Such power law behavior is typically associated with dynamic scaling of the structure factor of height–height correlations:

$$S(q_\parallel, t) \propto I_0 F\left(\frac{q_\parallel}{q_0}\right). \tag{5}$$

The individual GISAXS scans observed at 650 °C do exhibit dynamic scaling, as seen in the inset of figure 10.

Due to the power law behavior, the structure factor amplitude is expected to scale as $I_0 \sim t^m$, where the exponent m is the growth exponent. Figure 7(b) shows that at this temperature the peak intensity grows in a power law behavior with an exponent $m = 0.91 \pm 0.07$. This is comparable to the value of 1 seen for the case of Si without seeding [34]. The characteristic spatial length scales as $q_0 \sim t^{-n}$, where the exponent n is the coarsening exponent. Figure 7(a) shows that the characteristic wavenumber exhibits a continuous power law relaxation with an exponent of approximately 0.28 ± 0.10, slightly lower than the values of 0.34–0.4 observed for Si without seeding [34].

Analysis of the scaling relations shows that the surface roughness grows as t^β, with $\beta = m/2 - n$. The growth exponent β is found from the fits of the roughness evolution (as seen in figure 9(a)) and is approximately 0.18 ± 0.06, which is equal to the value obtained during the non-seeded bombardment [34]. Thus the seeding at this level does not change the fundamental behavior observed in surface morphology development during normal-incidence bombardment at high temperatures where the surface remains crystalline.

4. Discussion and conclusions

For off-axis low-energy Ar^+ bombardment of Si, at ion incidence angles $45° < \varphi < 60°$, we observe clear ripple formation, in contrast to the results of Frost *et al* [4] in which no nanostructure formation was observed in this range. The ripple formation kinetics reported here are in reasonable agreement with BH predictions, given the significant uncertainties in the values of the theoretical coefficients. Inclusion of an ion impact induced lateral

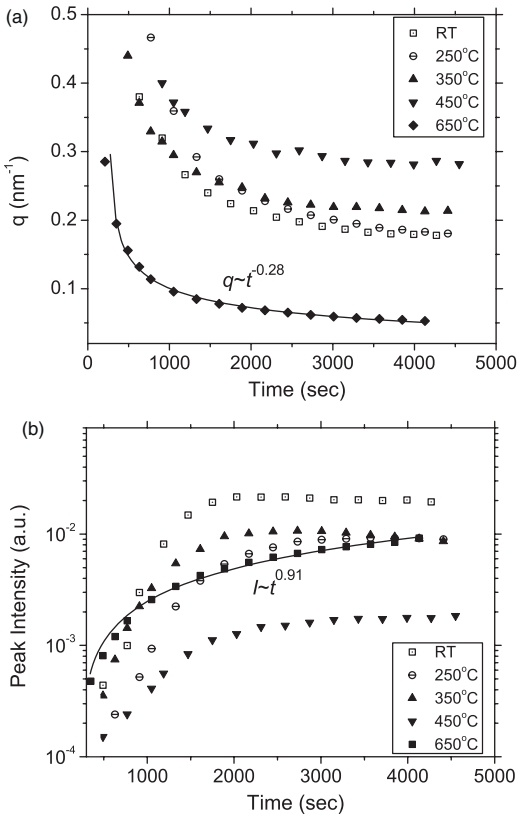

Figure 7. (a) Wavevector and (b) amplitude evolution of the correlation peaks of the samples bombarded at different temperatures.

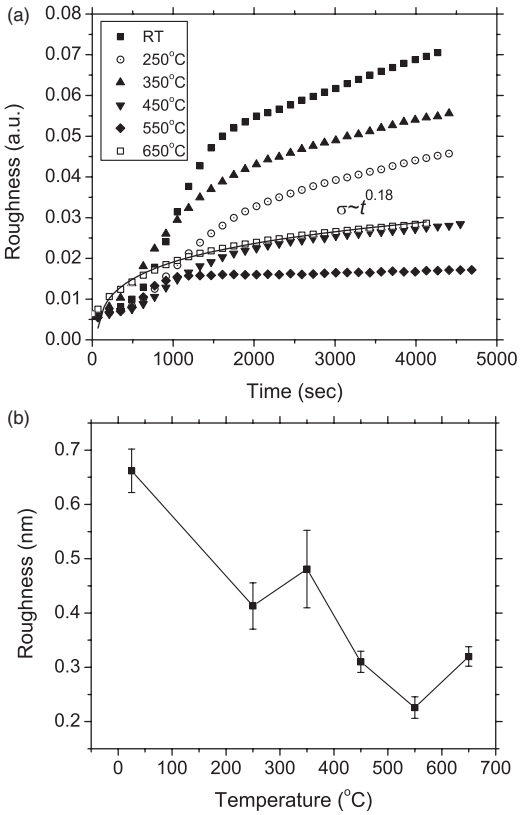

Figure 9. (a) Roughness evolution of the samples bombarded at different temperatures obtained from GISAXS scans and (b) final roughness values from *post facto* the AFM measurements.

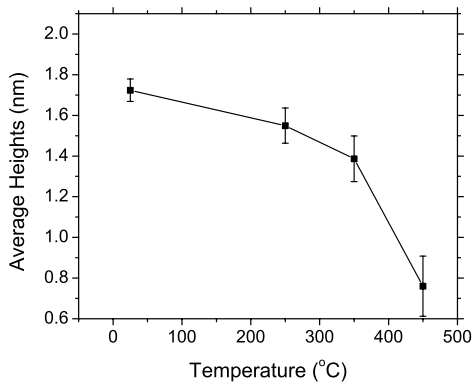

Figure 8. The final average heights of the nanodots obtained from the GISAXS data at different temperatures.

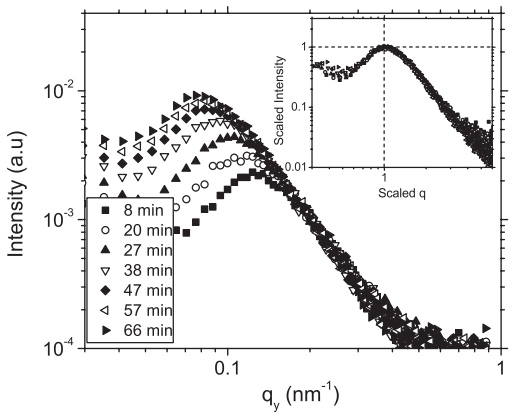

Figure 10. The GISAXS scans of sample bombarded at 650 °C. The inset shows GISAXS scans after scaling to peak position and amplitude.

mass redistribution term may explain the decrease in overall instability coefficient for smaller φ angles. However, there appears to be insufficient accuracy in calculations of the relevant coefficients using SRIM parameters to make definitive comparisons with experiment. The SES relaxation coefficient D_{yy} is comparable to, but smaller than, the overall observed relaxation coefficient which includes contributions from SD, SES and IVF. If IVF plays the dominant role, as seems likely from earlier work, the large surface viscosity η_s observed is consistent with an inverse relationship between η_s and ion flux.

The short wavelength smoothing observed during normal-incidence bombardment of pre-existing nanostructures is consistent with our previous report [6]. While there are also reports of native nanodot formation in such situations, recent concerns about inadvertent seeding suggest that this may play a role [9, 10]. On the other hand, Ziberi *et al* [36] have shown that the extent of ion beam divergence can affect the surface morphology development. In the future, we plan to characterize this issue with the Phi ion gun used in the native

studies. It should also be noted that ion impact induced lateral mass redistribution may lead to short length scale smoothing while nonlinearities lead to long length scale roughening, as observed in [6] and by Roy *et al* [37]. As is the situation for off-axis bombardment, more work is needed to better understand the diversity of results obtained by different groups for the native evolution of Si during low-energy bombardment.

Molybdenum seeding clearly has a major impact on morphology development—leading to the growth of nanodots—in the lower range of temperatures examined. It is notable, however, that figures 5–7 show that the average nanodot height and overall surface roughness decrease as temperature is increased. A similar trend with temperature was observed by Gago *et al* [38], though the presence or absence of seeding was not established explicitly there. This behavior is opposite to the reported effects of temperature on cone development in metals and also on microcone development for off-axis bombardment of Si with seeding. It suggests that the primary effect of thermal energy here is to aid surface relaxation mechanisms, rather than to promote the aggregation of seed atoms. If seed migration on the surface is relatively unimportant, then this may also suggest that the mechanism for nanodot growth is not the formation of protected regions by clusters of seed atoms. If nanodot formation is related instead to stress development on the surface [28], clustering of seed atoms might not be necessary.

At temperatures sufficiently high for the Si surface to remain crystalline (650 °C), it appears that seeding has little effect on the surface evolution during normal-incidence bombardment. Instead, as is the situation for the high temperature unseeded case, the dynamic scaling behavior of the structure factor suggests that an instability related to surface diffusion processes is responsible for the formation of rapidly coarsening nanoscale correlations.

Acknowledgments

We would like to thank E Anzenberg, P Siddons, H Zhou and R Headrick for their help, discussions and loan of a detector and the PHI ion gun. The work on seeded nanostructure development was supported by DOE DE-FG02-03ER46037 and the studies of native surface evolution were supported by NSF DMR-0507351. Data for this study were measured at beamline X21 of the National Synchrotron Light Source (NSLS). Financial support comes principally from the Offices of Biological and Environmental Research and of Basic Energy Sciences of the US Department of Energy.

References

[1] Guenterschulze A and Tollmien W V 1942 *Z. Phys.* **119** 685
[2] For a recent review, see Chan W L and Chason E 2007 *J. Appl. Phys.* **101** 121301
[3] Gago R, Vázquez L, Cueron R, Varela M, Ballesteros C and Albella J M 2001 *Appl. Phys. Lett.* **78** 3316
[4] Frost F, Ziberi B, Schindler A and Rauschenbach B 2008 *Appl. Phys.* A **91** 551
[5] Fan W, Ling L, Qi L, Li W, Sun H, Gu C, Zhao Y and Lu M 2006 *J. Phys.: Condens. Matter* **18** 3367
[6] Ozaydin G, Özcan A S, Wang Y, Ludwig K F, Zhao H, Headrick R L and Siddons D P 2005 *Appl. Phys. Lett.* **87** 163104
[7] Erlebacher J, Aziz M J, Chason E, Sinclair M B and Floro J A 1990 *Phys. Rev. Lett.* **82** 2330
[8] Keller A, Roßbach S, Facsko S and Möller W 2008 *Nanotechnology* **19** 135303
[9] Teichert C, Hofer C and Hlawacek G 2006 *Adv. Eng. Mater.* **8** 1057
[10] Sánchez-García J A, Vázquez L, Gago R, Redondo-Cubero A, Albella J M and Czigány Zs 2008 *Nanotechnology* **19** 355306
[11] Bradley R M and Harper J M E 1988 *J. Vac. Sci. Technol.* A **6** 2390
[12] Sigmund P 1973 *J. Mater. Sci.* **8** 1545
[13] Habenicht S, Bolse W, Lieb K, Reimann K and Geyer U 1999 *Phys. Rev.* B **60** R2200
[14] Alkemade P 2002 *Phys. Rev. Lett.* **96** 107602
[15] Davidovitch B, Aziz M J and Brenner M P 2007 *Phys. Rev.* B **76** 205420
[16] Kalyanasundaram N, Ghazisaeidi M, Freund J B and Johnson H T 2008 *Appl. Phys. Lett.* **92** 131909
[17] Carter G and Vishnyakov V 1996 *Phys. Rev.* B **54** 17647
[18] Moseler M, Gumbsch P, Casiraghi C, Ferrari A C and Robertson J 2005 *Science* **309** 1545
[19] Zhou H, Zhou L, Ozaydin G, Ludwig K F Jr and Headrick R L 2008 *Phys. Rev.* B **78** 165404
[20] Wehner G K and Hajicek D J 1970 *J. Appl. Phys.* **42** 1145
[21] Begrambekov L B, Zakharov A M and Telkovsky V G 1996 *Nucl. Instrum. Methods Phys. Res.* B **115** 456
[22] Fujimoto Y, Nozu M and Okuyama F 1995 *J. Appl. Phys.* **77** 2725
[23] Ma X L, Shang N G, Li Q, Lee C S, Bello I and Lee S T 2002 *J. Cryst. Growth* **234** 654
[24] Meng F Y, Wong W K, Shang N G, Li Q and Bello I 2002 *Vacuum* **66** 71
[25] Tanemura M, Yamauchi H, Yamane Y, Okita T and Tanemura S 2004 *Nucl. Instrum. Methods Phys. Res.* B **215** 137
[26] Tanemura M, Kobayashi M, Kudo M, Yammauchi H, Okita T, Miao L and Tanemura S 2006 *Surf. Sci.* **600** 3668
[27] Ozaydin G, Özcan A S, Wang Y, Ludwig K F, Zhou H and Headrick R L 2007 *Nucl. Instrum. Methods Phys. Res.* B **264** 47
[28] Ozaydin G, Ludwig K F Jr, Zhou H and Headrick R L 2008 *J. Vac. Sci. Technol.* B **26** 551
[29] Sinha S K, Sirota E B, Garoff S and Stanley H B 1998 *Phys. Rev.* B **38** 2297
[30] Makeev M A, Cuerno R and Barabási A-L 2002 *Nucl. Instrum. Methods Phys. Res.* B **197** 185
[31] Umbach C C, Headrick R L and Chang K C 2001 *Phys. Rev. Lett.* **87** 246104
[32] Makeev M A and Barabasi A-L 1997 *Appl. Phys. Lett.* **71** 2800
[33] Ziegler J F and Biersack J P *Computer Code SRIM-2008* http://www.srim.org.
[34] Ozaydin G, Ludwig K F Jr, Zhou H, Zhou L and Headrick R L 2008 *J. Appl. Phys.* **103** 033512
[35] Malis O, Brock J D, Headrick R L, Yi M-S and Pomeroy J M 2002 *Phys. Rev.* B **66** 035408
[36] Ziberi B, Frost F, Tartz M, Neumann H and Rauschenbach B 2004 *Thin Solid Films* **459** 106
[37] Roy A, Bhattacharjee K, Lenka H P, Mahapatra D P and Dev B N 2008 *Nucl. Instrum. Methods Phys. Res.* B **266** 1276
[38] Gago R, Vázquez L, Plantevin O, Sánchez-García J A, Varela M, Ballesteros M C, Albella J M and Metzger T H 2006 *Phys. Rev.* B **73** 155414